Report No. MDC 96K7062

A GENERAL INTERFACE METHOD FOR AEROELASTIC ANALYSIS OF AIRCRAFT

by

T. Tzong, H. H. Chen, K. C. Chang, T. Wu, T. Cebeci,

February 1996

Prepared Under
Contract No. NAS2-14091
for
NASA Ames Research Center

Report No. MDC 96K7062

A GENERAL INTERFACE METHOD FOR AEROELASTIC ANALYSIS OF AIRCRAFT

Issue date February 1996 **Contract number** NAS2-14091

Prepared by: T. Tzong
H. H. Chen
K. C. Chang
T. Wu
T. Cebeci

Approved by: T. Cebeci
MDC Distinguished Fellow

Summary

The aeroelastic analysis of an aircraft requires an accurate and efficient procedure to couple aerodynamics and structures. The procedure needs an interface method to bridge the gap between the aerodynamic and structural models in order to transform loads and displacements. Such an interface method is described in this report. This interface method transforms loads computed by any aerodynamic code to a structural finite element (FE) model and converts the displacements from the FE model to the aerodynamic model. The approach is based on FE technology in which virtual work is employed to transform the aerodynamic pressures into FE nodal forces. The displacements at the FE nodes are then converted back to aerodynamic grid points on the aircraft surface through the reciprocal theorem in structural engineering. The method allows both high and crude fidelities of both models and does not require an intermediate modeling. In addition, the method performs the conversion of loads and displacements directly between individual aerodynamic grid point and its corresponding structural finite element and, hence, is very efficient for large aircraft models.

This report also describes the application of this aero-structure interface method to a simple wing and an MD-90 wing. The results show that the aeroelastic effect is very important. For the simple wing, both linear and nonlinear approaches are used. In the linear approach, the deformation of the structural model is considered small, and the loads from the deformed aerodynamic model are applied to the original geometry of the structure. In the nonlinear approach, the geometry of the structure and its stiffness matrix are updated in every iteration and the increments of loads from the previous iteration are applied to the new structural geometry in order to compute the displacement increments. Additional studies to apply the aero-structure interaction procedure to more complicated geometry will be conducted in the second phase of the present contract.

1.0 INTRODUCTION

The aeroelastic analysis of an aircraft requires an accurate and efficient procedure to couple aerodynamics and structures. The procedure can be developed by using either a closely coupled approach in which the aerodynamic and structural equations are solved simultaneously, or a loosely coupled one, in which the loads computed with an aerodynamic model are transformed into a structural model for structural analysis, and the displacements resulting from the structural analysis are converted back to the aerodynamic model to update the geometry. The advantage of the closely coupled approach is that the results can be obtained with a single analysis. However, this advantage has three potential drawbacks: (1) an extensive code modification is required to couple any structural and aerodynamic codes and, hence, the evaluation of a new structural or aerodynamic code may be time-consuming and costly; (2) numerical problems in the solution of simultaneous equations including two disciplines may be difficult to resolve; and (3) including the aerodynamic grid deformation in the solution is rather involved and may require a major modification to the aerodynamic code. On the contrary, at a cost of a few iterations between aerodynamic and structural models to get converged solutions for loads and displacements, a general interaction procedure using the loosely coupled approach can be established. With this procedure, the aeroelastic analysis can be conducted with any aerodynamic and structural codes and require little modifications to either code. Therefore, a loosely coupled approach is adopted in this study.

In general, the aerodynamic and structural models are generated independently using different tools with differences in geometry. An interface method is required in order to transform the loads and displacements between the two models. In the structural design, the aeroelastic analysis is usually performed with a crude aerodynamic model, using linear aerodynamic method, and a high fidelity structural model. In the aerodynamic performance evaluation, a high fidelity aerodynamic model using advanced CFD code along with a crude structural model is employed. While both approaches can provide an accurate prediction of total loads, lift and drag for the entire aircraft, they may not provide accurate prediction of loads on aircraft components such as flaps, slats and spoilers. As a result, it is necessary to conduct flight tests. In addition, in structural design, the local loads (loads at finite element nodal points) are distributed from global loads according to a presumed pressure distribution. The global loads including shear, moment and torque at each wing section are computed using a simple beam model. Therefore, the local loads may not be accurate. From the above considerations, an interface method, which is suitable for both loads and performance evaluation of the entire aircraft as well as aircraft components and conserves local and global loads, is necessary.

Several interface methods have been developed for aeroelastic analysis [1-5]. Some of these methods, however, do not convert the local loads accurately for structural design.

Others either require an intermediate modeling between aerodynamic and structural models, which complicates the aeroelastic analysis, or have not been demonstrated for large aircraft models. Therefore, it is advantageous to have a method that transforms loads and deformations directly between large-order structural and aerodynamic models and is friendly to use.

In this report, an accurate and efficient interface method for transforming loads computed by any aerodynamic code to any structural finite element (FE) model and converting the displacements from the FE model to the aerodynamic model is described. The method allows both high and low fidelity models to be used. In addition, the method converts the loads and displacements directly between individual aerodynamic grid points and corresponding structural finite elements and, hence, is very efficient for large aircraft models.

The interface method is described in Section 2. An iteration procedure is developed to repeat calculations of loads and deformations in the aeroelastic analysis. In the procedure, a linear or a nonlinear approach can be used. In the linear approach, the deformation of the structural model is considered small and the loads from the deformed aerodynamic model are applied to the original geometry of the structure. On the other hand, in the nonlinear approach the geometry of the structure, and thus its stiffness matrix, is updated in every iteration, and the increments of loads from the previous iteration are applied to the new structural geometry to compute the displacement increments. The interface method has been integrated into a finite element code developed at McDonnell Douglas Corporation. Section 3 describes the application of the interface method to a simple wing and an MD-90 production wing. The aerodynamic pressures are computed using the OVERFLOW [6] code by solving the Navier-Stokes equations or a Douglas panel code [7]. Studies are conducted to examine the aeroelastic effect on the lift and drag of both wings. Conclusions and recommendations are made in Section 4.

2.0 INTERFACE METHOD

Different characteristics between aerodynamic and structural models influence the interface method for the conversion of the loads and deformations between the two models. The aerodynamic model generally includes details of the aircraft geometry, such as flaps, slats, pylon, nacelle, etc., and closely resembles to the true geometry of the aircraft. However, the FE model usually represents only major structural components. For example, the wing box, which carries major loads in the spanwise direction, is of main structural concern and is modeled in reasonable detail. The flaps and slats, which carry relatively small loads, are either represented by a few simple beam elements or completely excluded from the FE model. In addition, the engine and pylon are commonly modeled by a lumped (point) mass element and a general stiffness matrix, respectively, which do not resemble the true configurations of the components at all. Furthermore, tens of thousands aerodynamic grid points on the surface of an aircraft are usually needed to compute the pressure distribution. However, only hundreds or thousands of FE nodal points are used to model aircraft structures. The difference in fidelity between the two models results in gaps between the aerodynamic surface and the finite element surface. In order to accurately convert the loads and displacements, the inconsistency between the two models must be properly considered in the interface method.

The interface method developed in this report is based on FE technology in which the virtual work is employed to transform aerodynamic pressures into FE nodal forces. The displacements at FE nodes are then converted back to aerodynamic grid points on the aircraft surface through the reciprocal theorem in structural engineering.

There are two methods to convert loads between the aerodynamic and finite element models. One method is to convert the aerodynamic pressures to the FE model and the other is to convert the aerodynamic grid point forces on the aircraft surface. The forces are obtained by integrating pressures over the area surrounding the grid point. The inconsistency between the two models makes the pressure conversion improper. The pressures can be accurately converted from the aerodynamic model to the FE model. When the pressures are integrated, the information about the true surface areas may, however, not be available from the FE model. The area information can only be obtained from the aerodynamic model. Therefore, the approach undertaken herein is to convert integrated aerodynamic point forces to the finite element model.

The first step to perform aeroelastic analysis using the interface method is to project each aerodynamic grid point on the aircraft surface onto an adjacent finite element. The projection generates basic data to be used in the aero-structure interaction process. The data include the finite element projected by each aerodynamic grid point, the projected location of the aerodynamic grid point on the element and the offset distance from the aerodynamic grid point to the element surface. With this information, the displacements

at an aerodynamic grid point on the aircraft surface can be expressed in terms of the displacements at the projected location on the finite element surface as

$$\underline{u}_{aero} = \begin{Bmatrix} u \\ v \\ w \end{Bmatrix}_{aero} = \begin{bmatrix} 1 & & & & r_z & \\ & 1 & & -r_z & & \\ & & 1 & & & \end{bmatrix} \begin{Bmatrix} u \\ v \\ w \\ \theta_x \\ \theta_y \\ \theta_z \end{Bmatrix}_{FE} \tag{1}$$

where $\underline{u}_{aero}$ contains three translational displacement components at the aerodynamic grid point, and r_Z is the offset distance from the aerodynamic grid point to the element surface. The finite element displacements include both the translational degrees of freedom (DOF) u, v and w, and rotational DOF θ_x, θ_y and θ_z. However, membrane elements that are commonly used to represent skin, ribs and spars of aircraft wings do not have any rotational DOF at the FE nodal points. The translational displacements everywhere in the element can be defined by the nodal point displacements through element shape functions. The rotations at the projected location can be expressed by the differentials of the translational displacements as

$$\begin{Bmatrix} \theta_x \\ \theta_y \\ \theta_z \end{Bmatrix}_{FE} = \frac{1}{2} \begin{bmatrix} & -\frac{\partial}{\partial z} & \frac{\partial}{\partial y} \\ \frac{\partial}{\partial z} & & -\frac{\partial}{\partial x} \\ -\frac{\partial}{\partial y} & \frac{\partial}{\partial x} & \end{bmatrix} \begin{Bmatrix} u \\ v \\ w \end{Bmatrix}_{FE} \tag{2}$$

The displacements at each aerodynamic grid point are then expressed in terms of the translational displacement components at the projected location as

$$\underline{u}_{aero} = \begin{Bmatrix} u \\ v \\ w \end{Bmatrix}_{aero} = \frac{1}{2}\begin{bmatrix} 1 & & & r_z \\ & 1 & -r_z & \\ & & 1 & \end{bmatrix} \begin{bmatrix} 2 & & \\ & 2 & \\ & & 2 \\ & -\frac{\partial}{\partial z} & \frac{\partial}{\partial y} \\ \frac{\partial}{\partial z} & & -\frac{\partial}{\partial x} \\ -\frac{\partial}{\partial y} & \frac{\partial}{\partial x} & \end{bmatrix} \begin{Bmatrix} u \\ v \\ w \end{Bmatrix}_{FE} \tag{3}$$

By employing the reciprocal theorem, forces and moments at the projected location on the finite element surface can be written in terms of forces at the aerodynamic grid point as

$$\underline{p}_{FE} = \begin{Bmatrix} p_x \\ p_y \\ p_z \\ m_x \\ m_y \\ m_z \end{Bmatrix}_{FE} = \begin{bmatrix} 1 & & & \\ & 1 & & \\ & & 1 & \\ & & -r_z & \\ r_z & & & \end{bmatrix} \begin{Bmatrix} p_x \\ p_y \\ p_z \end{Bmatrix}_{aero} \tag{4}$$

where $\underline{p}_{FE}$ is the force vector on the finite element surface and $\underline{p}_{aero} = \{p_x \; p_y \; p_z\}^T_{aero}$ is the force at the aerodynamic grid point obtained by integrating aerodynamic pressures over the area surrounding the point. In the above equation, the moments due to the offset distance r_z from the aerodynamic grid point to the element surface and the inplane force components p_x and p_y are conserved. In addition, the offset can properly transform the aerodynamic forces on aircraft components that are excluded from the finite element model.

2.1 Finite Element Forces by Virtual Work

The virtual work in the finite element formulation can be expressed as

$$W = \int \delta \underline{u}^T_{FE} \underline{p}_{FE} dA = \delta \underline{U}^T \underline{F} \tag{5}$$

where W is the virtual work, $\underline{F}$ and $\underline{U}$ are the finite element nodal forces and displacements, respectively, $\underline{p}_{FE}$ and $\underline{u}_{FE}$ are the load and displacement vectors at any point on the element surfaces, and A is the surface area of the structure subjected to aerodynamic pressures. $\underline{u}_{FE} = \{u\ v\ w\ \theta_x\ \theta_y\ \theta_z\}^T_{FE}$ contains both the translational and rotational displacement components.

With the introduction of the finite element shape functions, Eq. (5) can be written as

$$W = \delta \underline{U}^T \left[\int \left(\underline{N}^T \bar{\underline{p}}_{FE} + \nabla \underline{N}^T \bar{\underline{m}}_{FE} \right) dA \right] \tag{6}$$

where $\bar{\underline{p}}_{FE}$ and $\bar{\underline{m}}_{FE}$ denote the distributed forces and moments at any location on the element surface , respectively, and $\bar{\underline{p}}_{FE} = \{p_x\ p_y\ p_z\}^T$ and $\bar{\underline{m}}_{FE} = \{m_x\ m_y\ m_z\}^T$. $\underline{\mathrm{N}}$ is the matrix of the element shape functions, and $\nabla \underline{N}$ is the differential of the shape functions $\underline{N}$. The translational displacements at any location on the element surface are

$$\bar{\underline{u}}_{FE} = \underline{N}\underline{U} = \sum_i \begin{bmatrix} N_i & & \\ & N_i & \\ & & N_i \end{bmatrix} \begin{Bmatrix} U \\ V \\ W \end{Bmatrix}_i \tag{7}$$

The rotations at any location are given by

$$\bar{\underline{\theta}}_{FE} = \nabla \underline{N}\underline{U} = \frac{1}{2} \sum_i \begin{bmatrix} & -\partial N_i/\partial z & \partial N_i/\partial y \\ \partial N_i/\partial z & & -\partial N_i/\partial x \\ -\partial N_i/\partial y & \partial N_i/\partial x & \end{bmatrix} \begin{Bmatrix} U \\ V \\ W \end{Bmatrix}_i \tag{8}$$

where $\{U\ V\ W\}^T_i$ are the displacements at the ith node of the finite element model.

From Eqs. (5) and (6), the finite element nodal forces are found to be

$$\underline{F} = \int \left(\underline{N}^T \bar{\underline{p}}_{FE} + \nabla \underline{N}^T \bar{\underline{m}}_{FE} \right) dA \tag{9}$$

In terms of forces and moments projected from the aerodynamic grid point to the finite element surface, the above equation can be written as

$$\underline{F} = \sum_{j=1}^{M} \left(\underline{N}^T(\xi_j, \eta_j) \bar{\underline{p}}_{FE_j} + \nabla \underline{N}^T(\xi_j, \eta_j) \bar{\underline{m}}_{FE_j} \right) \tag{10}$$

where ξ_j and η_j denote the coordinates of the projected location of the jth aerodynamic grid point on a finite element, $\bar{\underline{p}}_{FE_j}$ and $\bar{\underline{m}}_{FE_j}$ denote the corresponding finite element forces and moments converted from the aerodynamic point forces by Eq. (4), and M denote the total number of aerodynamic grid points on the aircraft surface. The calculation of coordinates of the projected location on finite elements is given in Appendix A.

After the load vector is formed, the displacements at finite element nodes can be obtained with the structural stiffness matrix. The displacements at aerodynamic grid points are then computed by Eq. (3). An algorithm for the calculation of the projection of each aerodynamic grid point on a finite element and loads and displacements conversion is given in Appendix B.

2.2 Linear and Nonlinear Approaches

There are two approaches to perform the aero-structure interaction: the linear approach and the nonlinear approach. In the beginning of the aero-structure interaction, the aerodynamic loads on the rigid wing are calculated first and applied to the finite element model in order to compute the elastic deformation. A modified wing geometry is then obtained by superimposing the elastic deformation on the rigid wing geometry. The next iteration is performed by calculating the aerodynamic loads based on the modified wing geometry due to deformation. If the elastic deformation is small, the stiffness of the finite element model changes slightly with the geometry. In the linear approach, the stiffness of the deformed wing is assumed to be the same as that of the rigid wing, and the aerodynamic loads based on the modified wing geometry are applied to the original finite element model in order to compute a new elastic deformation. This deformation is then superimposed on the rigid wing to determine an updated wing geometry for the next iteration. This iteration procedure is repeated until both loads and deformations converge. In the nonlinear approach, the stiffness and the geometry of the finite element model are updated in every iteration in order to take the geometric nonlinear effects into account. An iteration procedure similar to the linear approach is used. However, aerodynamic loads applied to the deformed finite element model are the increments of the loads from the previous iteration.

In this report both approaches are used with an underrelaxation parameter to accelerate the convergence of the iterations. In the nonlinear approach, a smaller relaxation parameter is used, which corresponds to smaller increments in loads between two iterations.

3.0 RESULTS

To demonstrate the aero-structure interface procedure, two wings have been studied. The first corresponds to a simple swept wing with a constant cross section of a NACA 0012 airfoil. The aspect ratio and sweep angle are 3.5 and 30°, respectively. This wing has been tested for both subsonic and transonic flows. The second wing is the MD-90 wing at cruise conditions.

3.1 Simple Wing at Transonic Flow Conditions

The structural model of the simple wing contains only the wing box, which is modeled by membrane and rod elements. The finite element model composed of 97 nodes, 211 elements and 209 degrees of freedom is shown in Figure 1. The leading and trailing edges of the wing are excluded from the finite element model in order to demonstrate the aero-structure interface procedure. Choosing $M_\infty = 0.8, Re = 21X10^6$ and $\alpha = 3°$, the aerodynamic pressure distribution on the surface of the wing is calculated with the OVERFLOW [6] code which uses the Baldwin-Barth turbulence model. The C-O type field grid is generated with 145X29X49 grid points. The CPU time for each run of the OVERFLOW code is approximately one hour on CRAY C-90 with the current grid. Since a smaller relaxation parameter is used in the nonlinear approach, more iterations are required for the solutions to converge. To save computer time, the aero-structure interaction analysis for the simple wing at transonic flow conditions is performed with the linear approach only. For a relaxation parameter of 0.7, four iterations were required for both loads and deformations to converge within one percent tolerance.

The aerodynamic pressure is integrated over the area of each mesh and distributed to corner points of the mesh to obtain the forces at each grid point of the aerodynamic model. The aerodynamic loads on the wing are then converted into loads at the nodal points of the finite element model. Figure 2 shows the forces at each grid point of the aerodynamic model and the converted loads at each node of the finite element model, respectively. As can be seen, the nodal forces on the finite element model vary uniformly and the local force distributions are realistic and reasonable. The calculations also show that the total lift and moment are conserved through the conversion from the aerodynamic model to the finite element model.

Figure 3 shows the rigid and deformed wing geometry based on the aerodynamic model, and Figure 4 shows the same geometry with the region near the wing tip enlarged. The smoothness of the geometry shown in both figures demonstrates that the present aero-structure interface procedures is functioning well.

Figure 5 shows the pressure contours of the rigid and deformed wings. Figure 6 shows the net aerodynamic forces (the difference between the forces on the upper and lower surfaces) at each grid point of the aerodynamic model for both rigid and deformed wings. Figure 7 shows the pressure distributions at four different spanwise locations for both rigid and deformed wings. As can be seen, the shock location moves forward and the net aerodynamic loads are reduced as the wing deforms. The amount of the reduction of the net aerodynamic load is greater at the outboard of the wing than that at the inboard of the wing. Figures 8(a) and 8(b) show the elastic deflection at the trailing edge and the twist angle of the deformed wing along the span, respectively. The maximum deflection is 17.15 inches, which is 4.9 percent of the span and occurs at the tip trailing edge. The twist angle is defined as the difference between the leading edge and trailing edge deflections divided by the chord. As can be seen, the twist angle increases along the spanwise direction and approaches an asymptotic value near the wing tip. Figures 8(c) and 8(d) show the shear force and the integrated bending moment distributions along the span for both rigid and deformed wings. The results show that the shear force at the wing root has been reduced by 22 percent, and the bending moment at the wing root has been reduced by 24 percent due to the elastic deformation.

Table 1 shows the aeroelastic effects on the aerodynamic performance. Both lift and drag coefficients of the simple wing at transonic flow conditions are reduced by more than twenty percent due to the deformation. The results indicate that the aeroelastic effects are important and should not be neglected.

Table 1. The aeroelastic effects on the simple wing at transonic flow conditions

NACA 0012 Wing, M_∞=0.8, Re=21x10^6, α=3°

Iteration No.	$C\ell$	Percentage of Change in $C\ell$	C_d	Percentage of Change in C_d
1	.2746		.01349	
2	.2130	-22.4	.01039	-23.0
3	.2135	-22.2	.01020	-24.4
4	.2144	-21.9	.01019	-24.5

3.2. Simple Wing at Subsonic Flow Conditions

It is more efficient to use a panel method to calculate the aerodynamic pressure distributions in order to study both linear and nonlinear approaches for the aero-structure interaction and to evaluate the geometric nonlinear effects due to the elastic deformation. For this purpose we use the Douglas panel method due to Hess [7] and compute the

pressure distributions for angles of attack of $\alpha = 2^\circ$ and $\alpha = 8^\circ$. In the linear approach, a relaxation parameter 0.7 is used in every iteration. In the nonlinear approach, different relaxation parameters are used. To ensure accuracy, iterations are repeated until both loads and deformations converge to the fourth digit. With this convergence criterion, seven iterations are required in the linear approach for both angles of attack. In the nonlinear approach for $\alpha = 2^\circ$, seven iterations are required for a relaxation parameter of 0.7 and fifteen iterations are required for a relaxation parameter of 0.1 initially and gradually increasing to 0.7. For $\alpha = 8^\circ$, the calculations require twenty-eight iterations for a relaxation parameter of 0.05 initially and gradually increasing to 0.7.

Figure 9 shows the aerodynamic forces at each grid point of the aerodynamic model for $\alpha = 8^\circ$. It is seen that the load distributions are uniform along the spanwise direction. Figure 10 shows the net aerodynamic forces at each grid point for both rigid and deformed wings. It is seen that the net aerodynamic loads have been reduced more near the tip region as the wing deforms. Figure 11(a) and 11(b) show the elastic deflection at the trailing edge and the twist angle of the deformed wing along the span at $\alpha = 2^\circ$. The maximum deflection is 8.31 inches based on the linear approach, 8.45 inches based on the nonlinear approach with a relaxation parameter of 0.7, and 8.58 inches based on the nonlinear approach with an initial relaxation parameter of 0.1, respectively. As can be seen, the geometric nonlinear effect of the structural model tends to increase the elastic deformation of the wing. However, the differences between the results are not significant, and the results indicate that it is not necessary to use the nonlinear approach for the simple wing at subsonic flow conditions.

Figure 11(c) and 11(d) show the shear force and the integrated bending moment distributions along the span for both rigid and deformed wings at $\alpha = 2^\circ$. The results based on linear and nonlinear approaches are very close to each other. The shear force and bending moment at the root are reduced by more than 15 and 21 percent due to deformation, respectively. Figure 12 shows similar results to those in Figure 11 for $\alpha = 8^\circ$. The maximum deflection is 32.36 inches based on the linear approach and 33.36 inches based on the nonlinear approach. The shear force at the wing root is reduced by more than 14 percent and the bending moment is reduced by more than 20 percent due to deformation. The results again indicate that the nonlinear effects are not significant.

Table 2 shows the aeroelastic effects for the simple wing at subsonic flow conditions. The results indicate that the lift coefficient is reduced by about twenty percent for both $\alpha = 2^\circ$ and 8°.

Table 2. The aeroelastic effects on the simple wing at subsonic flow conditions

NACA 0012 Wing, α=2°

	C_ℓ	Percentage of Change
Rigid wing	.1613	
Deformed wing, linear, rel = 0.7	.1308	-18.9
Deformed wing, nonlinear, rel = 0.7	.1294	-19.8
Deformed wing, nonlinear, rel = 0.1	.1284	-20.4

NACA 0012 Wing, α=8°

	C_ℓ	Percentage of Change
Rigid wing	.6409	
Deformed wing, linear	.5250	-18.1
Deformed wing, nonlinear,	.5127	-20.0

3.3. MD-90 Wing at Cruise Conditions

An original and a modified finite element models for the MD-90 wing are shown in Figure 13. The original finite element model containing the wing box and simplified leading and trailing edge devices were generated for production structural analysis. The skin, ribs and spars in the wing box are modeled by membrane elements and stringers by beam and rod elements. The leading and trailing edges, including flaps, slats, etc., are simplified with beam elements which are not shown in the figure. The beam elements provide proper mechanisms to transfer loads from leading and trailing edges to the wing box. This model is modified to perform the aero-structure interaction analysis. Dummy membrane elements (with zero stiffness and mass) are added to the leading and trailing edges in order to properly convert loads from the aerodynamic model into the finite element model. The modified finite element model is composed of 4,558 nodes, 12,177 elements and 25,323 degrees of freedom.

The pressure distributions on the surface of this wing were obtained with the OVERFLOW code for cruise conditions at 31,000 ft with $M_\infty = 0.76$ and $\alpha = 2°$. The C-O type field grid contained 225X49X49 grid points. Since approximately two hours of CRAY C-90 CPU time are required for each run of the OVERFLOW code with the current grid, only the linear approach is used to perform the aero-structure interface procedure. For a relaxation parameter of 0.7, four iterations are required for the loads and deformations to converge within one percent tolerance. Figure 14 shows the aerodynamic

forces on the aerodynamic and the finite element models, respectively. Figure 15 shows the rigid and deformed wing geometry based on the aerodynamic model.

Figure 16 shows the pressure contours, and Figure 17 shows the pressure distributions at four different spanwise locations for both rigid and deformed wings. As can be seen, the aerodynamic pressures near the wing root remain almost the same and the shock location changes slightly except near the wing tip. The suction peak becomes smaller near the tip region as the wing deforms. Figures 18(a) and 18(b) show the trailing edge deflection and the elastic twist angle of the MD-90 wing along the span, respectively. The maximum deflection occurs at the tip trailing edge and is 19.27 inches, which is only 1.5 percent of the span. As can be seen, the twist angle increases along the spanwise direction until it reaches maximum value near the wing tip and then begins to decrease. This is different from the results for the simple wing. Figures 18(c) and 18(d) show the shear force and the integrated bending moment distributions along the span for both rigid and deformed wings. Since the MD-90 wing only deforms slightly at the cruise conditions, the reduction of the shear force and bending moment due to the elastic deformation is insignificant. The lift of the wing is reduced by less than three percent which indicates that the aeroelastic effects for the MD-90 wing at the cruise conditions are not significant.

4.0 CONCLUSIONS

A general interface method for aeroelastic analysis of aircraft has been developed. The method can be used with any aerodynamic and structural code and is applicable to any aircraft configuration. It does not require additional input besides the aerodynamic and finite element models and is very efficient for large aircraft models.

The interface method has been tested for a simple wing and an MD-90 production wing. The results for the simple wing show that the aeroelastic effects are very important. A reduction of more than twenty percent in lift and drag coefficients has been observed. However, the aeroelastic effects are not so significant for the MD-90 wing, and there is less than three percent reduction in lift for the cruise conditions. Since the MD-90 wing is designed for critical loads, it is relatively stiff for the cruise conditions. In addition, the wing's chord is tapered down from the inboard of the wing to the outboard. Therefore, the deflection at the outboard wing does not reduce lift and drag as much as those for the constant-chord simple wing model.

Both linear and a nonlinear iteration procedures for aeroelasticity have also been studied. Results from the linear approach differ from those of the nonlinear approach by approximately three percent. However, in the large aircraft structural design, three percent reduction in loads and, hence, three percent savings in structural materials is significant. In addition, the difference between linear and nonlinear approaches may be higher if complex geometries such as wing/fuselage/nacelle/pylon are considered. Further studies by applying the aero-structure interaction procedure to more complex geometries are necessary.

During the study of the MD-90 wing model, it was found that spanwise separation between aircraft components such as flaps and other control surfaces influences the calculations. The separation is a result of structural deformation. The difficulty resides in the aerodynamic calculation, which requires grids to bridge the gaps between flaps and control surfaces in order to obtain accurate pressure distributions. An improved grid generator is therefore needed to solve this problem.

Aircraft trim analysis, which balances the aircraft payload by lift and determines its angle of attack and flap rotations, is important to the loads calculation. In production, the analysis is generally conducted with linear aerodynamic codes with an assumption that the aircraft deflection is a linear combination of pre-selected shapes. The production analysis, however, does not include the nonlinearity of aerodynamics and relies on wind tunnel test data to correct the results. With the general aeroelastic analysis method described here, more accurate trim analysis can be performed with advanced aerodynamic codes since the nonlinearity of aerodynamics is automatically included.

Appendix A

Projection of Aerodynamic Grid Points on Finite Elements

An important step in the interface method for aeroelastic analysis is to find the finite element and the projected location associated with each aerodynamic grid point. The search for the element in a three dimensional space requires that the distances between the aerodynamic grid points and finite elements as well as the normal direction of finite elements be known. The projected location of an aerodynamic grid point on the finite element surface can be defined by the local coordinates of the element. QUAD4 (a 4-node quadrilateral element) and TRIA3 (a 3-node triangular element) are two types of finite elements most commonly used to model aircraft surfaces. For QUAD4, the projected location can be found using the isoparametric shape functions of the element. The coordinates of the projected location can be written as

$$\begin{aligned} x &= \sum_{i=1}^{4} N_i(\xi,\eta)x_i \\ y &= \sum_{i=1}^{4} N_i(\xi,\eta)y_i \end{aligned} \tag{A-1}$$

where

$$N_1 = \frac{(1+\xi)(1+\eta)}{4},$$

$$N_2 = \frac{(1-\xi)(1+\eta)}{4},$$

$$N_3 = \frac{(1-\xi)(1-\eta)}{4},$$

$$N_4 = \frac{(1+\xi)(1-\eta)}{4},$$

and x_i and y_i are the ith nodal coordinates of the element, which are rotated and shifted from the global coordinate system to the element surface. ξ and η denote the local

coordinates and x and y denote the rotated and shifted global coordinates of the projected location.

A quadratic equation to find ξ can be written as

$$(a_2b_4 - a_4b_2)\xi^2 + [(a_2b_3 - a_3b_2) + (a_1b_4 - a_4b_1) + (ya_4 - xb_4)]\xi + (a_1b_3 - a_3b_1) + (ya_3 - xb_3) = 0 \tag{A-2}$$

where

$$a_1 = \frac{x_1 + x_2 + x_3 + x_4}{4}, \quad a_2 = \frac{x_1 - x_2 - x_3 + x_4}{4}$$
$$a_3 = \frac{x_1 + x_2 - x_3 - x_4}{4}, \quad a_4 = \frac{x_1 - x_2 + x_3 - x_4}{4}$$
$$b_1 = \frac{y_1 + y_2 + y_3 + y_4}{4}, \quad b_2 = \frac{y_1 - y_2 - y_3 + y_4}{4}$$
$$b_3 = \frac{y_1 + y_2 - y_3 - y_4}{4}, \quad b_4 = \frac{y_1 - y_2 + y_3 - y_4}{4}$$

Similarly, η can be computed from

$$(a_3b_4 - a_4b_3)\eta^2 + [(a_3b_2 - a_2b_3) + (a_1b_4 - a_4b_1) + (ya_4 - xb_4)]\eta + (a_1b_2 - a_2b_1) + (ya_2 - xb_2) = 0 \tag{A-3}$$

Both Eqs. (A-2) and (A-3) lead to two (may be identical) or, sometimes, no real solution. When there is no solution, the aerodynamic grid point is being extrapolated to a finite element with trapezoidal shape and unequal side lengths. Transformation of such elements into the local coordinate system results in a distorted solution domain which has a vacuum region where no real values of ξ and η can be found. In this case, the element is excluded from the selection of projection. If an element is the one which the aerodynamic grid point is projected onto, there are two sets of roots from the above two equations. However, only one set of ξ and η with reasonable magnitudes is selected. If an aerodynamic grid point is projected within an element boundary, both ξ and η are between -1 and 1.

The local coordinates of the projected location for an aerodynamic grid point on a TRIA3 element can be found using the element shape functions as

$$x = \sum_{i=1}^{3} L_i x_i$$
$$y = \sum_{i=1}^{3} L_i y_i \tag{A-4}$$

where L_i is the area coordinate of ith node of the TRIA3 element and $L_3 = 1 - L_1 - L_2$. The local coordinates of the projected location for an aerodynamic grid point can be obtained by solving the simultaneous equations as

$$(x_1 - x_3)L_1 + (x_2 - x_3)L_2 = x - x_3$$
$$(y_1 - y_3)L_1 + (y_2 - y_3)L_2 = y - y_3 \tag{A-5}$$

Appendix B

Algorithm for the Interface Method

The algorithm to determine the finite element projected by each aerodynamic grid point and the loads and displacement conversion are summarized below.

(1) Aerodynamic Grid Point Projection

- Find the normal direction of the aircraft surface at each aerodynamic grid point.

- Search for the FE projected by each aerodynamic grid point by projecting the point to each candidate FE and selecting the most proper one. The details of selecting the finite element are described in the following:

  (i) Find a few FE nodes closest to the aerodynamic grid point.
  (ii) Find all finite elements attached to the FE nodes. (Only QUAD4 and TRIA3 elements on the structure's surface are chosen.)
  (iii) Find the local element coordinates of the aerodynamic grid point on each candidate element. An extrapolation beyond element boundary may be needed.
  (iv) Select the finite element by (a) discarding the element whose surface normal forms an obtuse angle with the surface normal of the aerodynamic grid point; (b) choosing an element with the element coordinates of the projected location between -1 and +1 or a minimum extrapolation of coordinates; or (c) choosing the element with a minimum offset distance.
  (v) Save the local coordinates of the projected location, the offset distance between the aerodynamic grid point and the finite element.

(2) Loads Conversion

- Integrate pressures in each aerodynamic mesh into loads and distribute them to the attached aerodynamic grid points. The loads are in the global coordinate system with x, y and z components.

- Rotate and project the loads at each aerodynamic grid point to the QUAD4 or TRIA3 finite element. Perform the virtual work to obtain the loads at FE nodal points. Rotate the FE nodal loads to the global coordinate system and assemble them into the global load vector for the finite element solution.

(3) Displacements Conversion

With the finite element solution, the displacements at each aerodynamic grid point can be obtained as follows:

- Rotate the FE global displacements to the local element coordinate system. Interpolate or extrapolate the finite element nodal displacements to the aerodynamic grid point. (The displacements due to local rotation and offset distance are automatically included.) Rotate the displacements at aerodynamic grid points to the global coordinate system.

References

1. Harder, R., and Desmarais, R., "Interpolation Using Surface Splines," *Journal of Aircraft,* Vol. 9, No. 2, February, 1972, pp. 189-191.

2. Kroll, R., and Hirayama, M., "Modal Interpolation Program, L215 (INTERP), Volume I: Engineering and Usage," NASA Contractor Report 2847, 1979.

3. Guruswamy, G., and Byun, C., "Direct Coupling of Euler Flow Equations with Plate Finite Element Structures," *AIAA Journal*, Vol. 33, No. 2, April 1994, pp. 374-377.

4. Byun, C., and Guruswamy, G., "Wing-Body Aeroelasticity Using Finite-Difference Fluid/Finite-Element Structural Equations on Parallel Computers," AIAA-94-1487, *AIAA/ASME/ASCE/AHS/ASC, 35th Structures, Structural Dynamics, and Materials Conferences*, Hilton Head, South Carolina, April, 1994.

5. MacMurdy, D., Kapania, R., and Guruswamy, G., "Static Aeroelastic Analysis of Wings Using Euler/Navier-Stokes Equations Coupled with Improved Wing-box Finite Element Structures," AIAA-94-1587, *AIAA/ASME/ASCE/AHS/ASC, 35th Structures, Structural Dynamics, and Materials Conferences*, Hilton Head, South Carolina, April, 1994.

6. Buning, P. G., Chan, W. M., Renze, K., J., Sondak, D., Chiu, I. T., and Slotnick, J. P., "OVERFLOW User's Manual, Version 1.6," NASA Ames Research Center, Moffett Field, CA, 1991.

7. Hess, J. L., Friedman, D. M., and Clark, R. W., "Calculation of Compressible Flow About Three-Dimensional Inlets with Auxiliary Inlets, Slats and Vanes by Means of a Panel Method," NASA Contractor Report 174975, 1985.

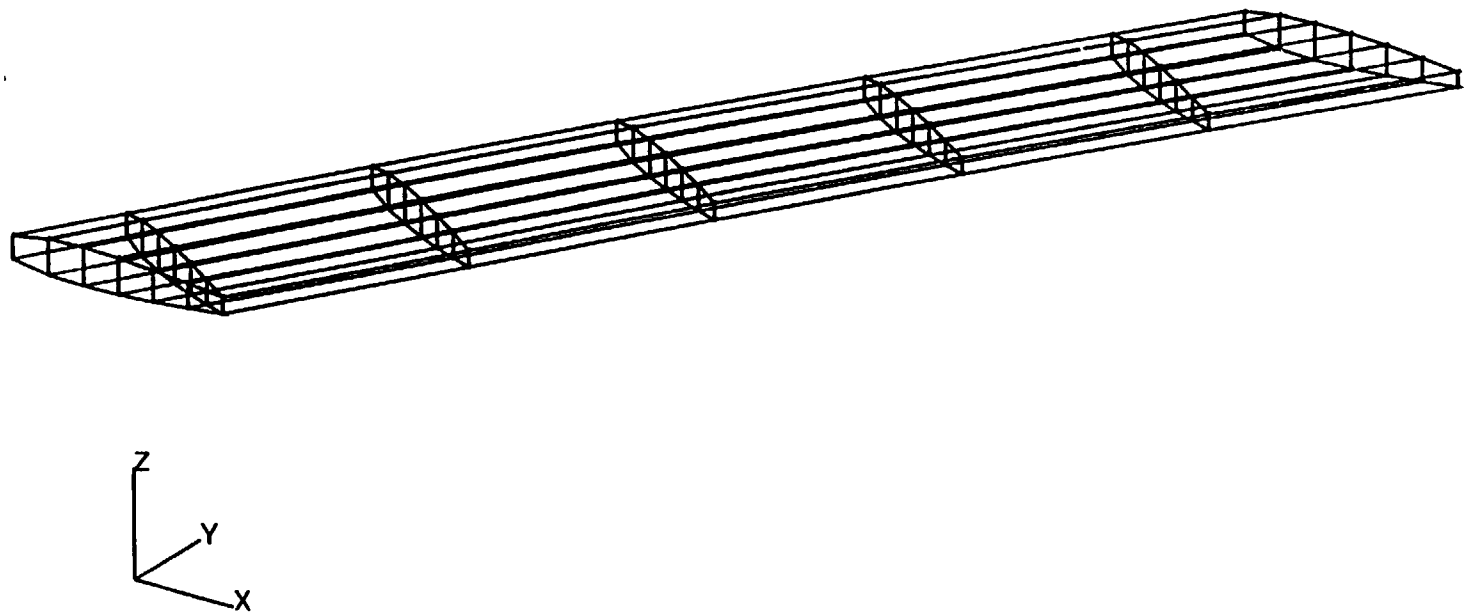

Figure 1. The finite element model of the simple wing

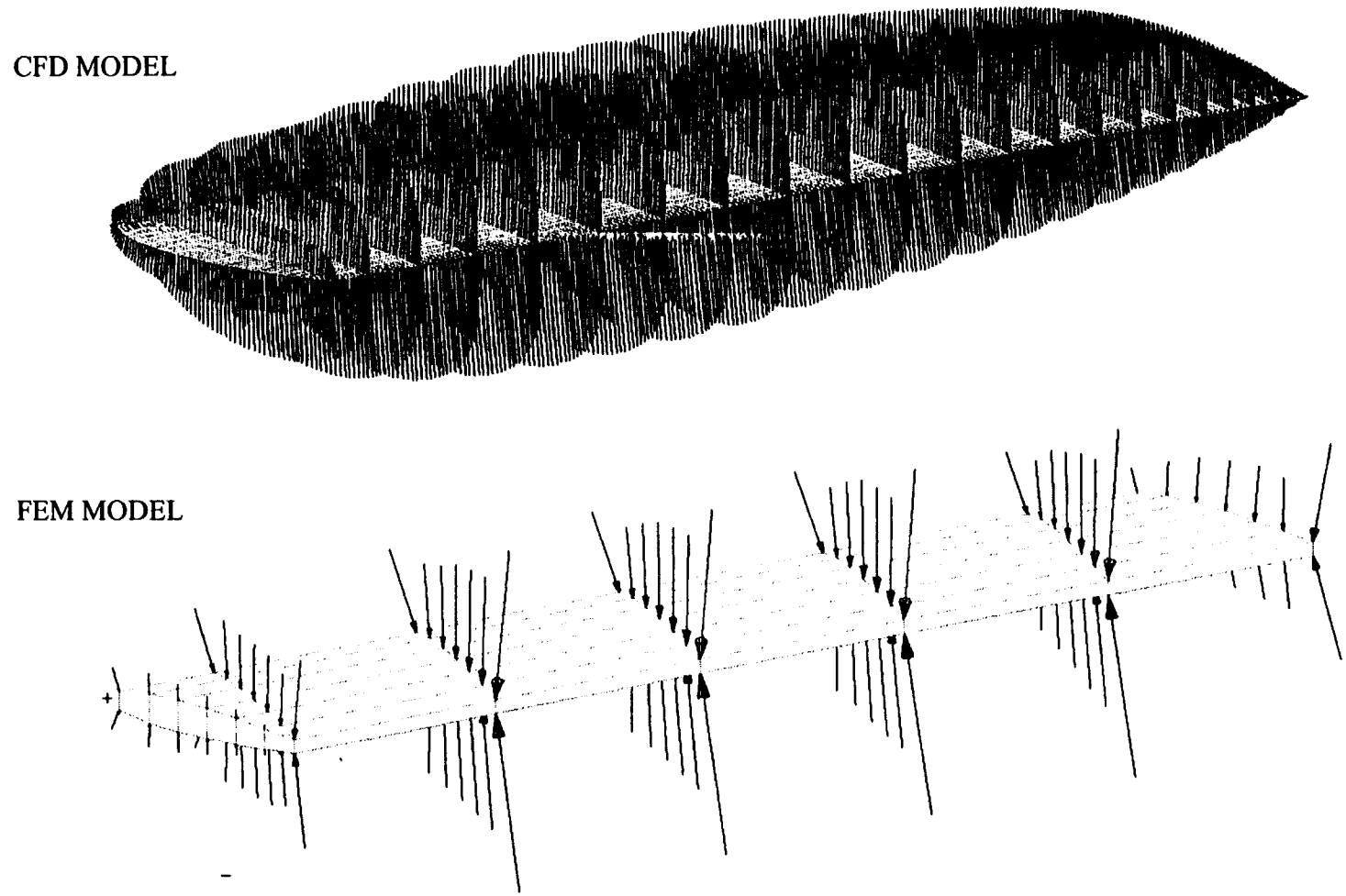

Figure 2. The aerodynamic loads on the simple wing at $M_\infty = 0.8, \mathrm{Re} = 21 \times 10^6$ and $\alpha = 3°$

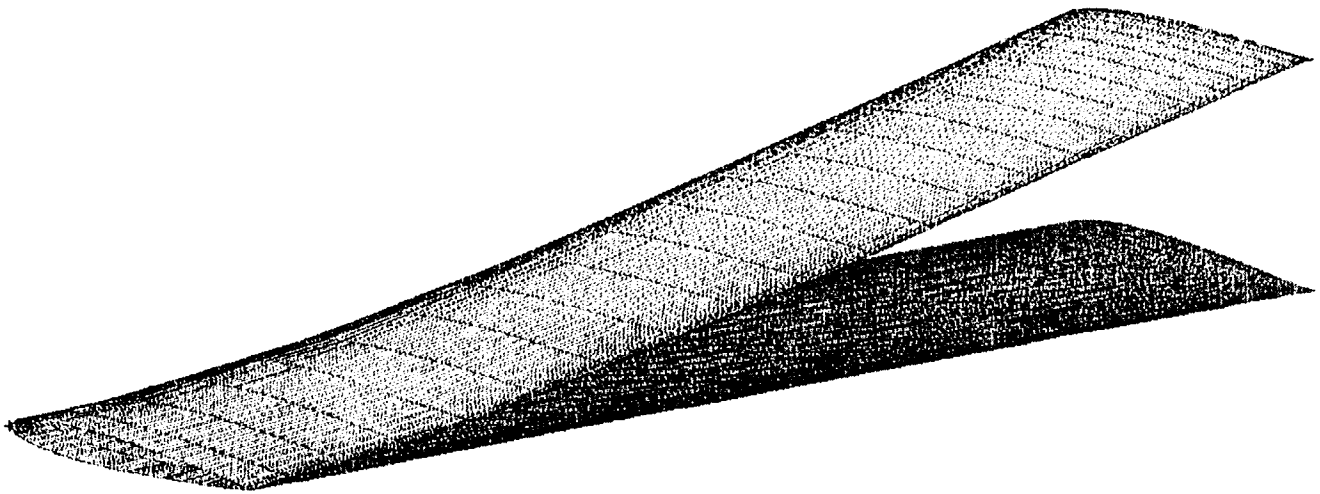

Figure 3. The rigid and deformed geometry of the simple wing at $M_\infty = 0.8, Re = 21 \times 10^6$ and $\alpha = 3^\circ$

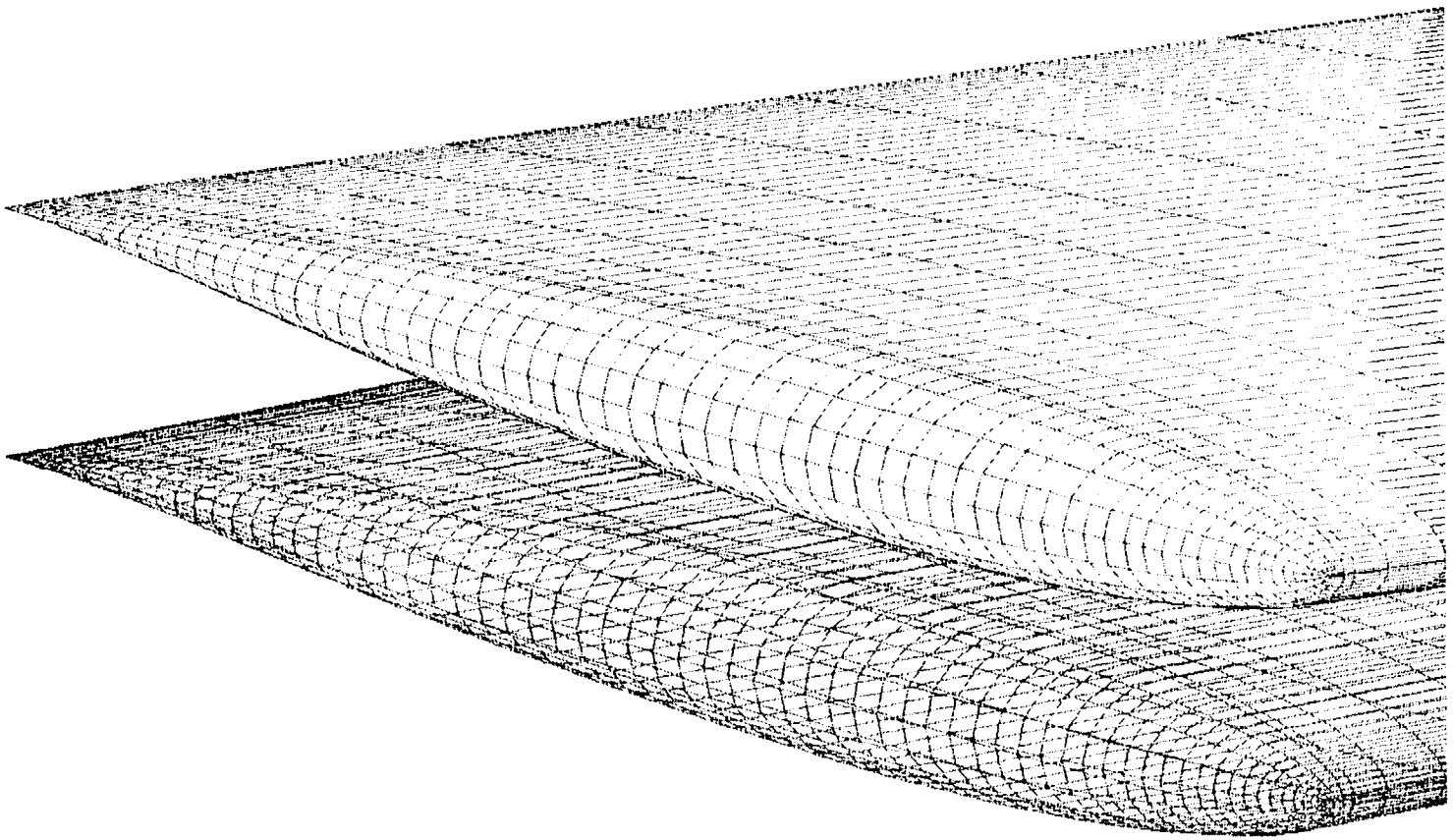

Figure 4. The rigid and deformed geometry at the tip of the simple wing at $M_\infty = 0.8, Re = 21 \times 10^6$ and $\alpha = 3^\circ$

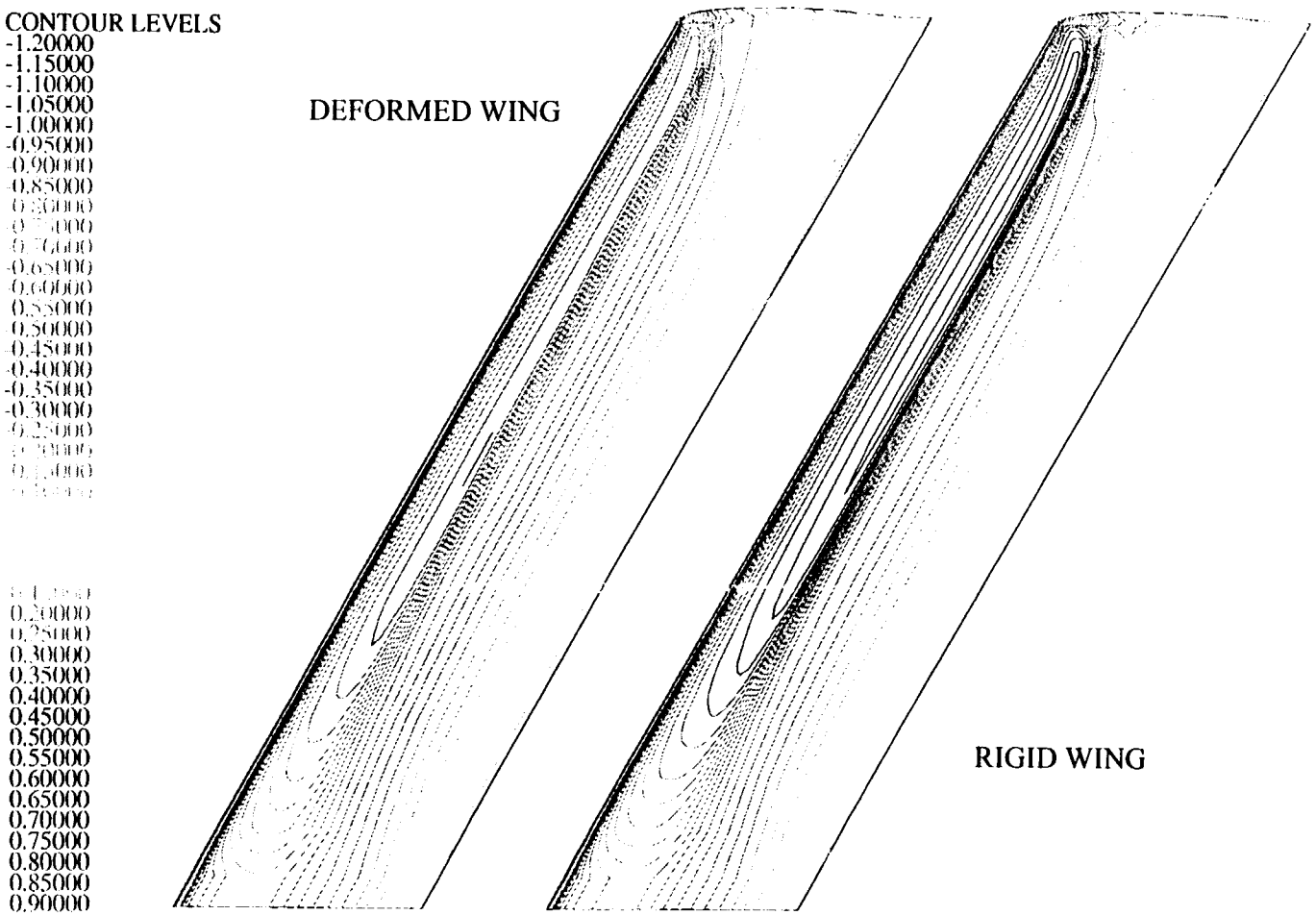

Figure 5. The pressure contours of the simple wing at $M_\infty = 0.8, Re = 21 \times 10^6$ and $\alpha = 3^\circ$

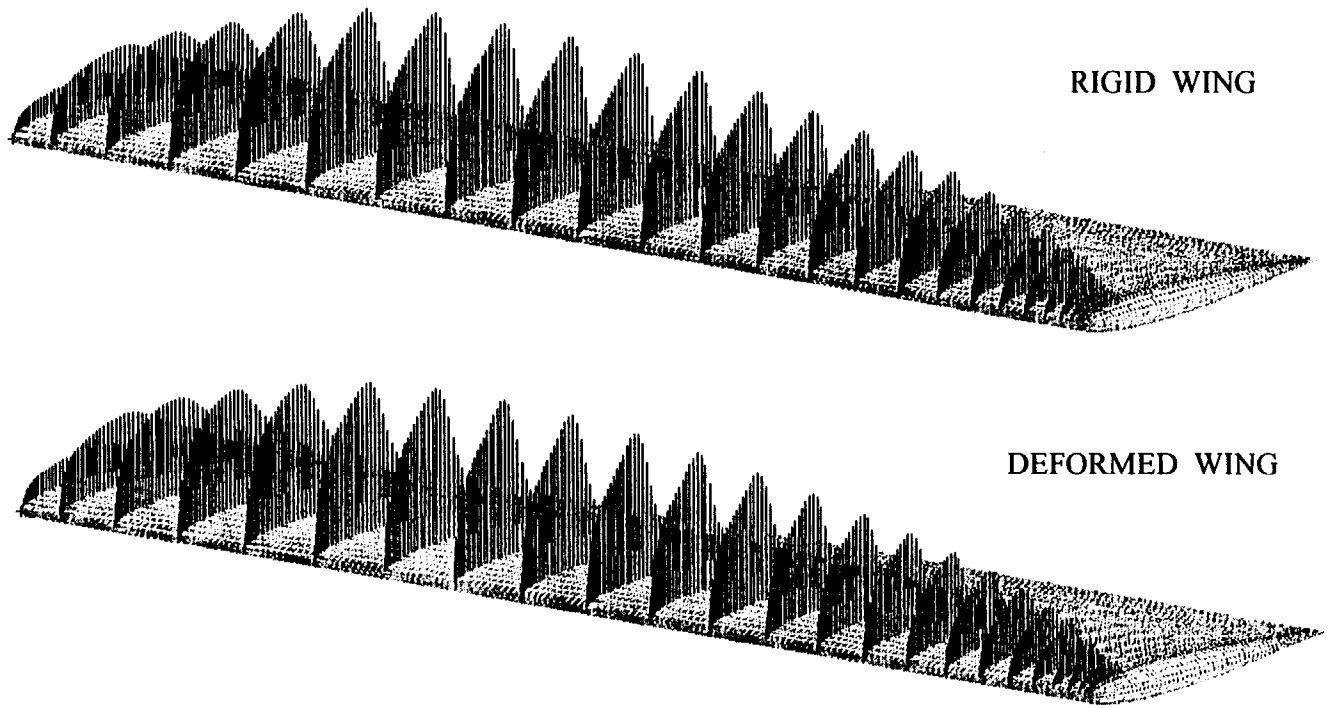

Figure 6. The net aerodynamic loads on the simple wing at $M_\infty = 0.8, Re = 21 \times 10^6$ and $\alpha = 3^\circ$

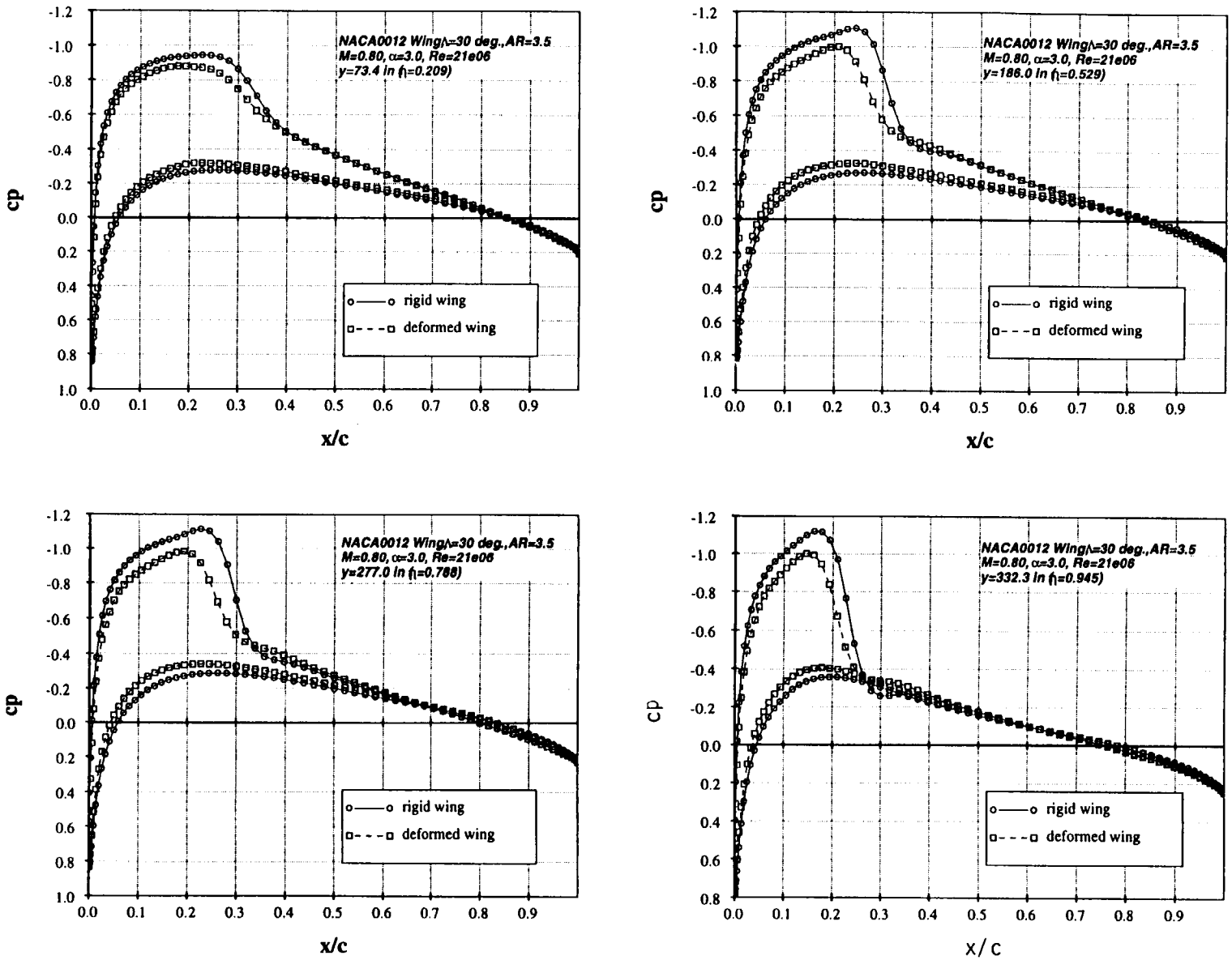

Figure 7. The pressure distributions at four spanwise locations of the simple wing at transonic speed

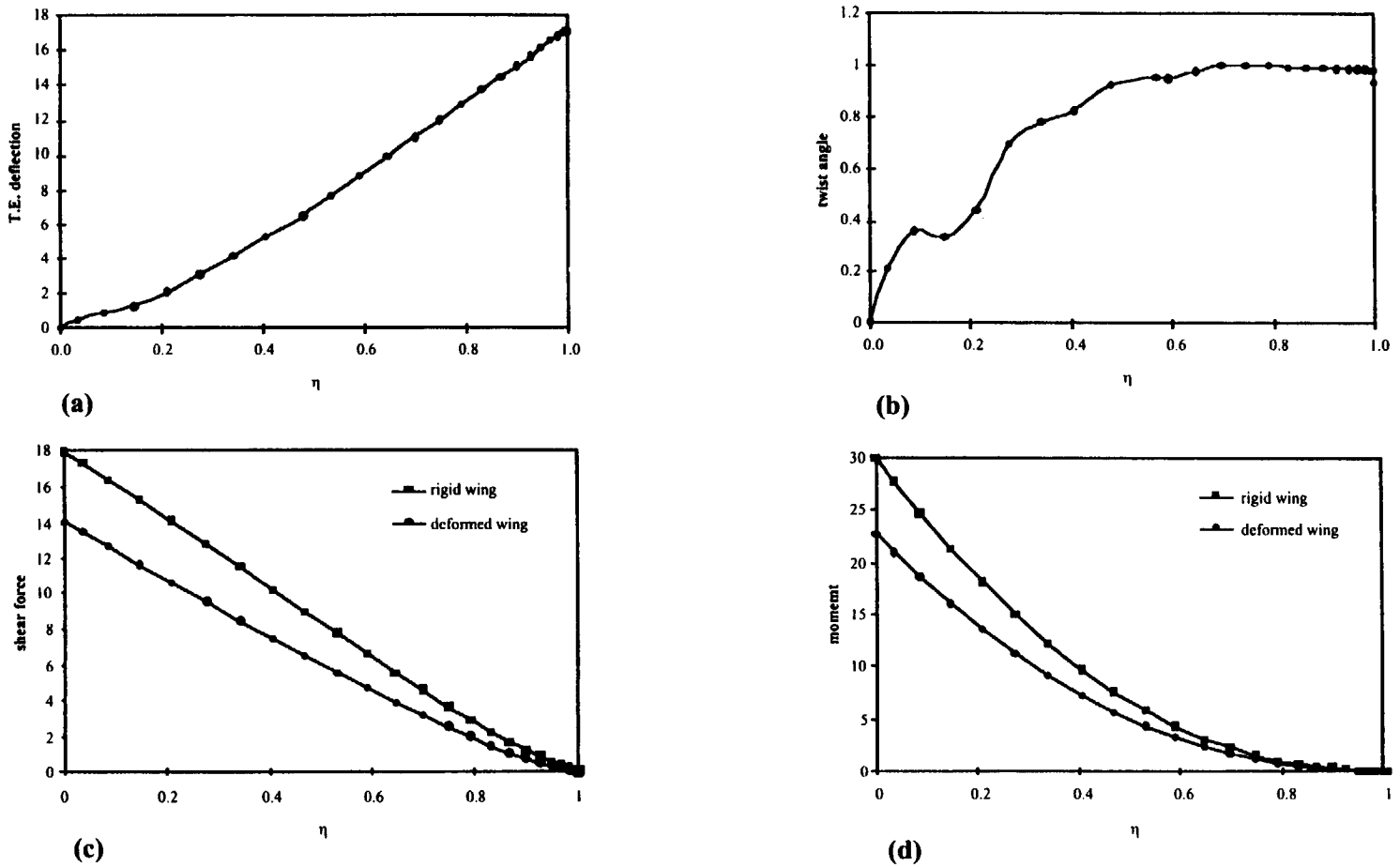

Figure 8. (a) The trailing edge deflection (b) the elastic twist angle (c) the shear force distribution and (d) the bending moment distribution of the simple wing at $M_\infty = 0.8, Re = 21 \times 10^6$ and $\alpha = 3^\circ$

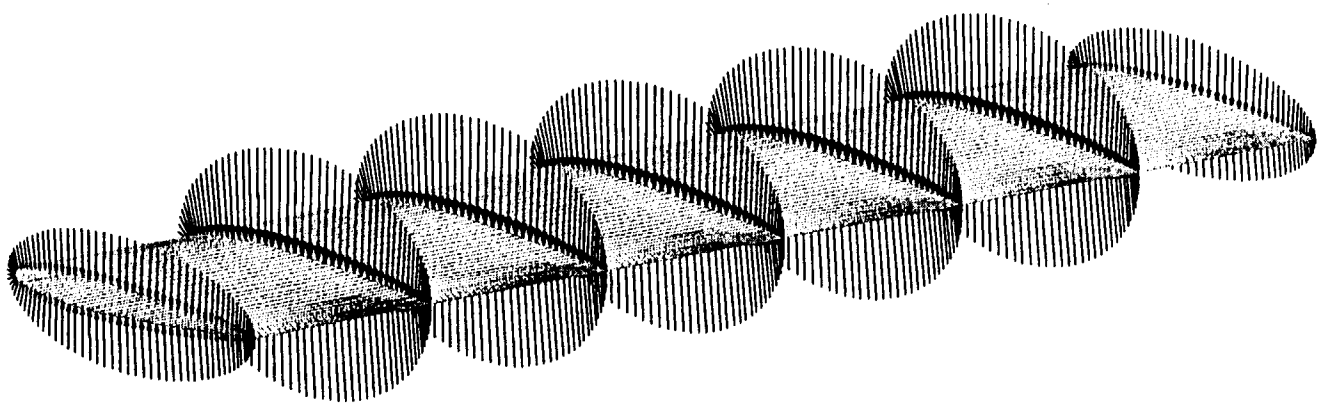

Figure 9. The aerodynamic loads on the simple wing at subsonic speed for $\alpha = 8^{\circ}$

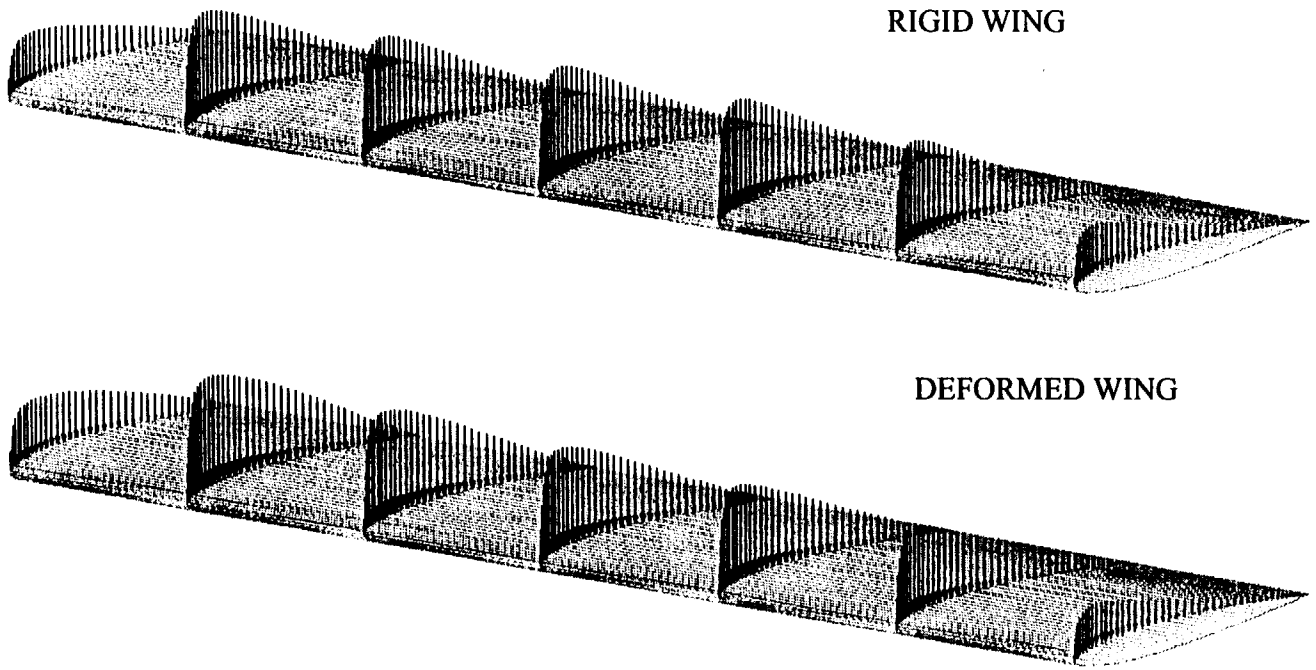

Figure 10. The net aerodynamic loads on the simple wing at subsonic speed for $\alpha = 8^{\circ}$

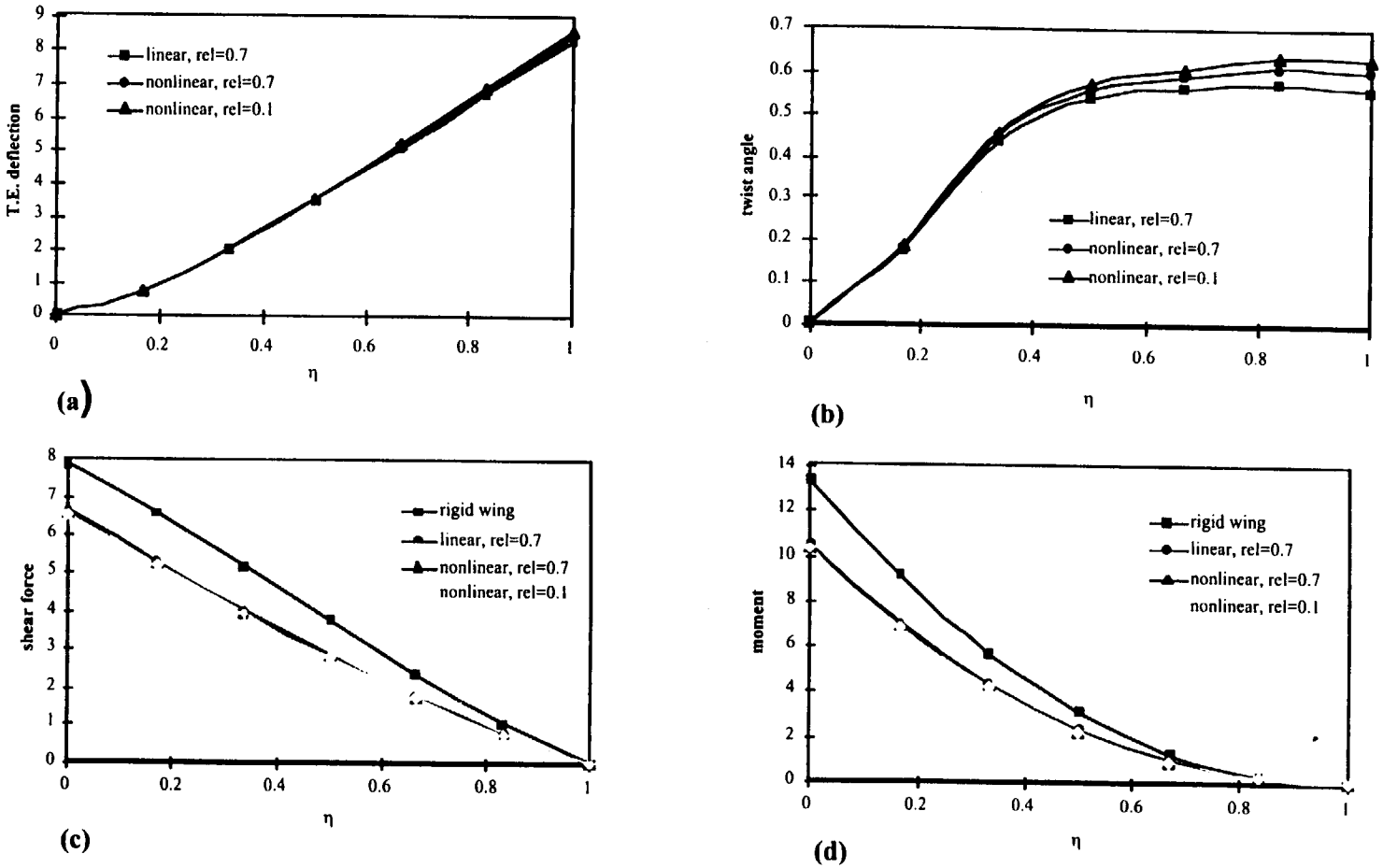

Figure 11. (a) The trailing edge deflection (b) the elastic twist angle (c) the shear force distribution and (d) the bending moment distribution of the simple wing at subsonic speed for $\alpha = 2^{\circ}$

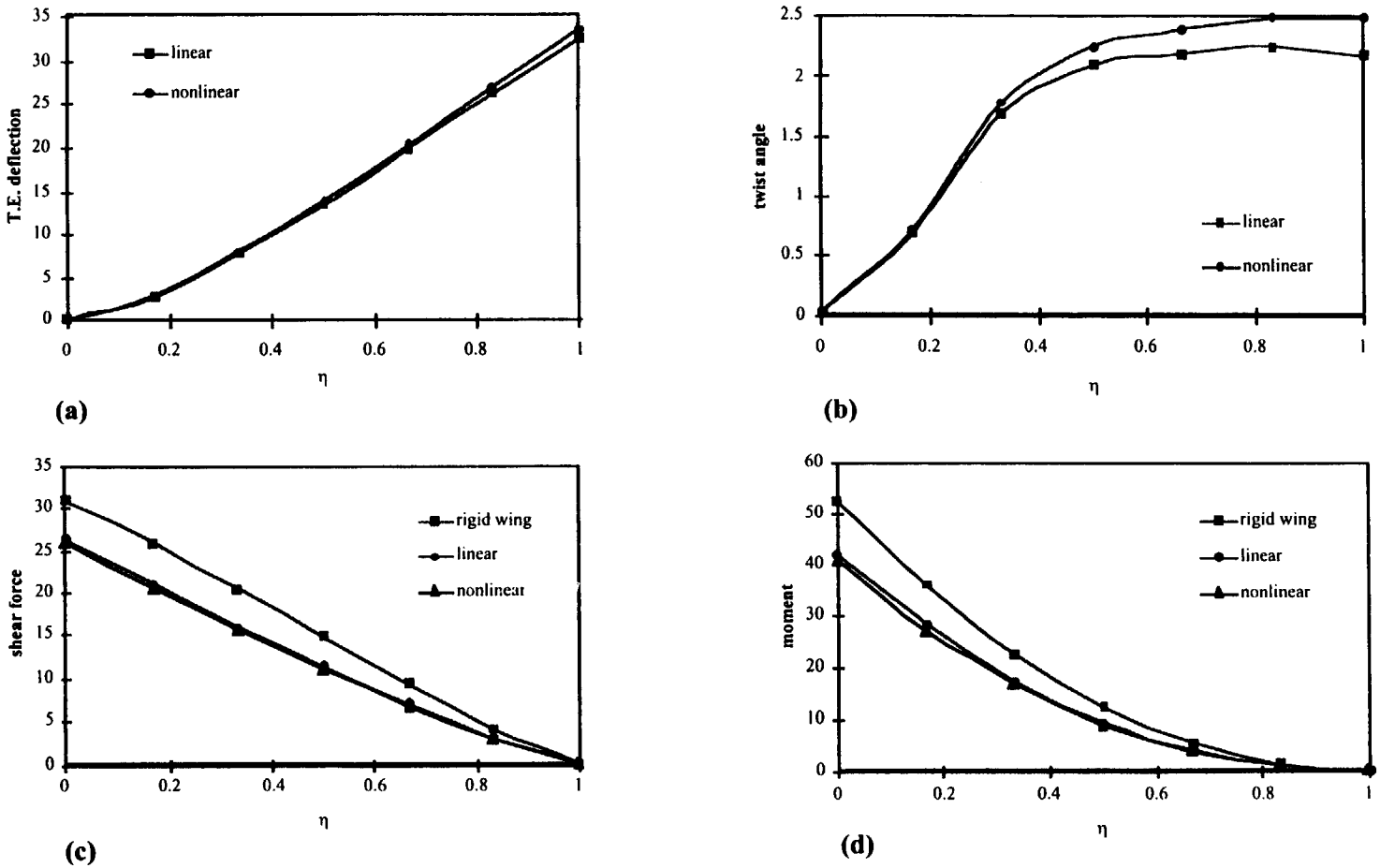

Figure 12. (a) The trailing edge deflection (b) the elastic twist angle (c) the shear force distribution and (d) the bending moment distribution of the simple wing at subsonic speed for $\alpha = 8^{\circ}$

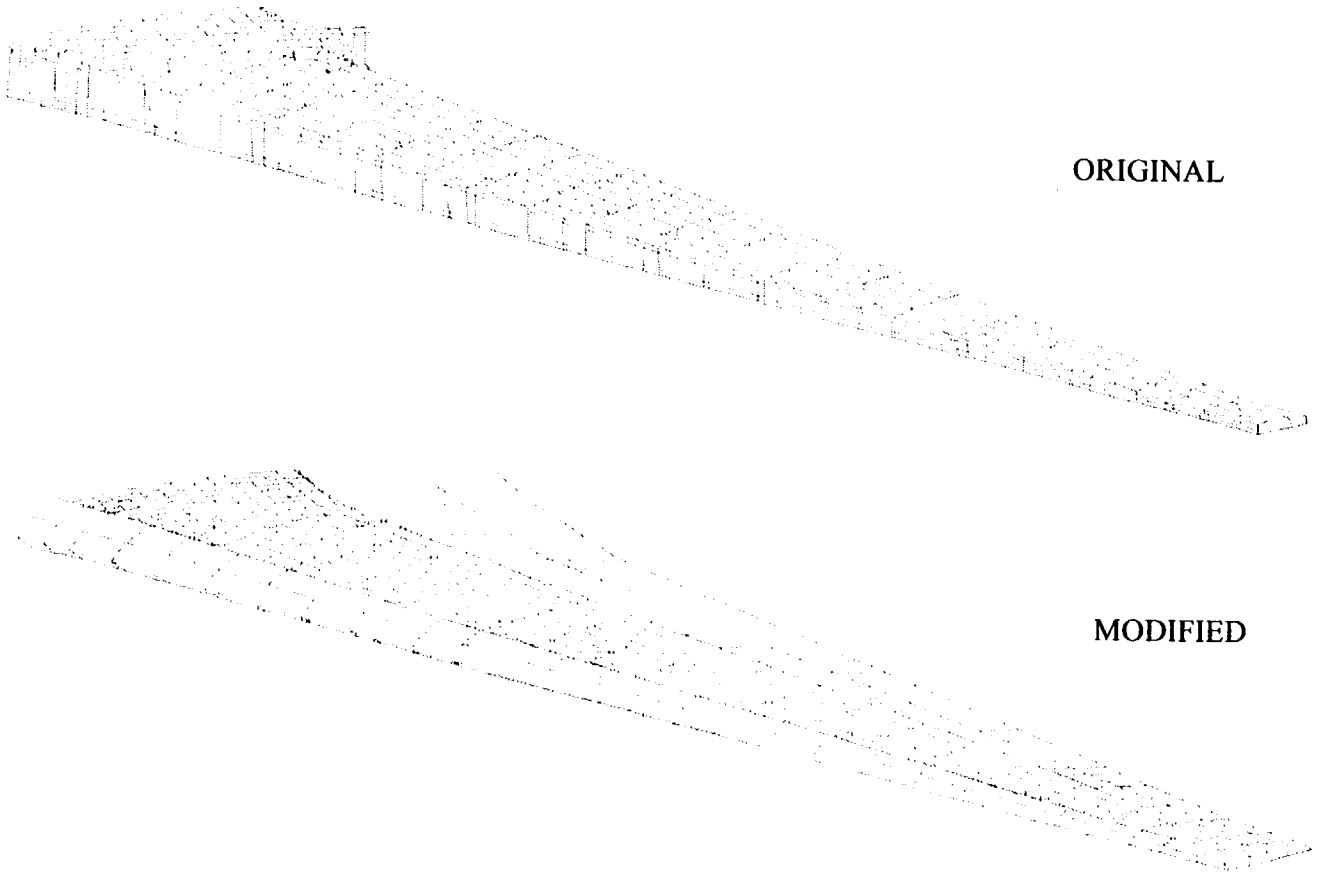

Figure 13. The finite element models for the MD-90 wing

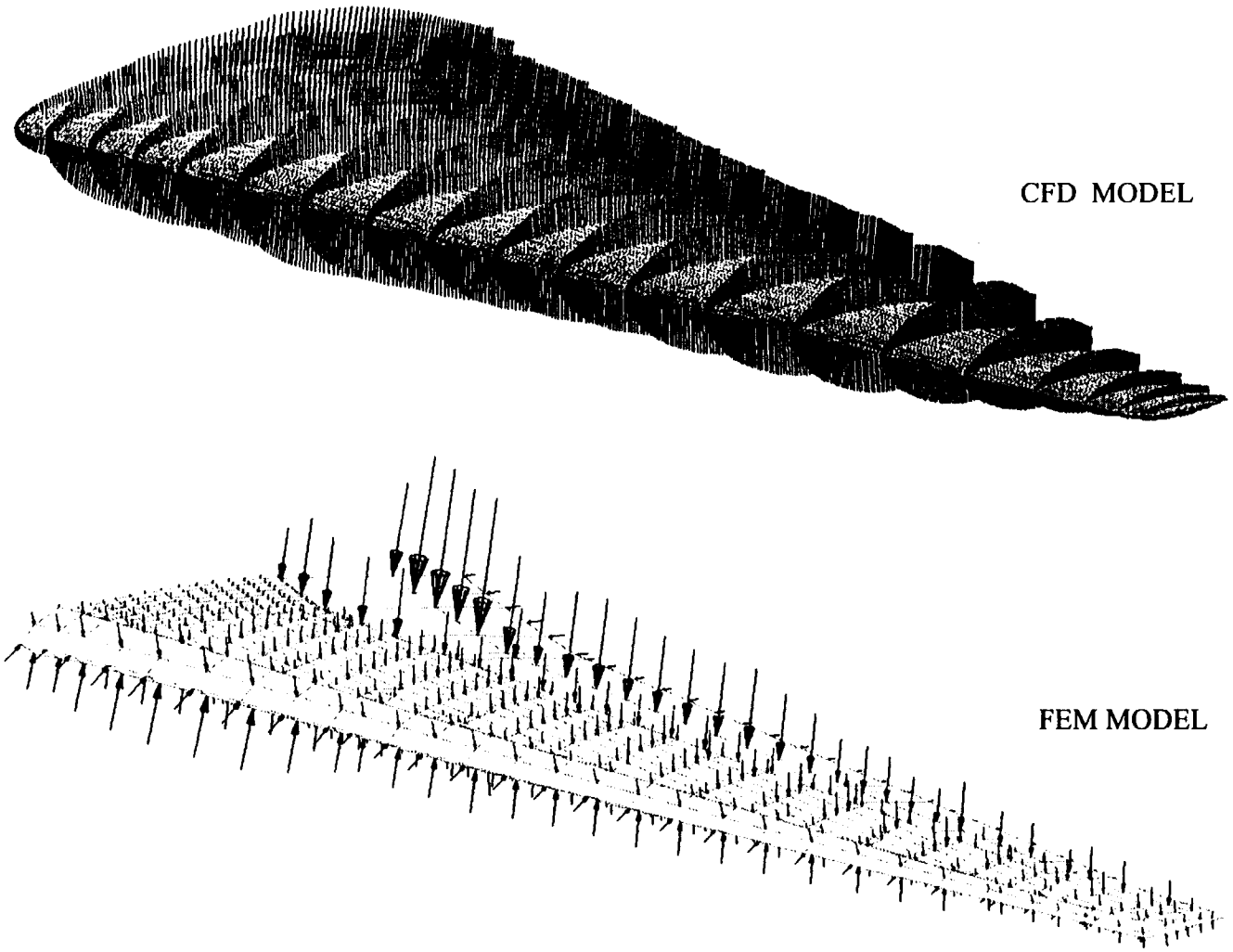

Figure 14. The aerodynamic loads on the MD-90 wing under the cruise condition

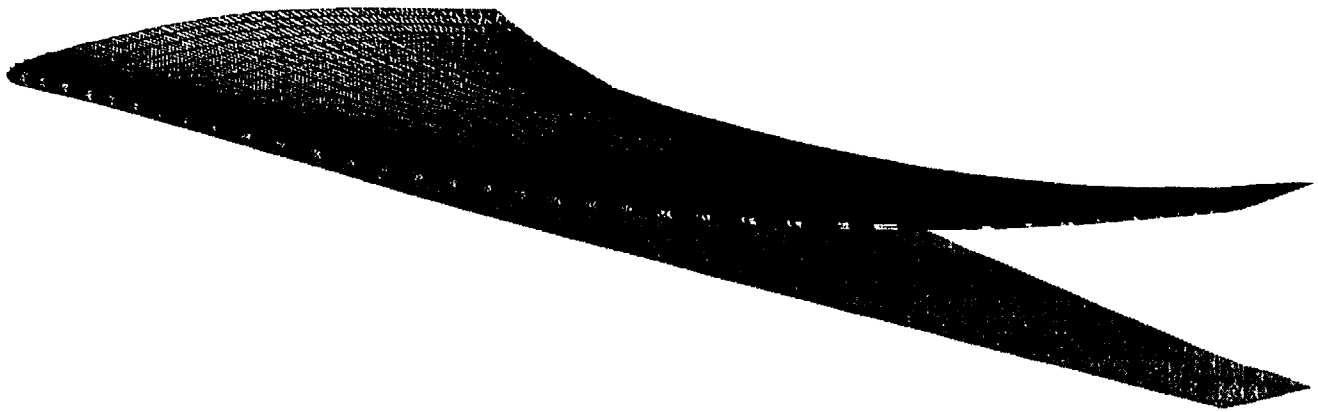

Figure 15. The rigid and deformed geometry of the MD-90 wing under the cruise condition

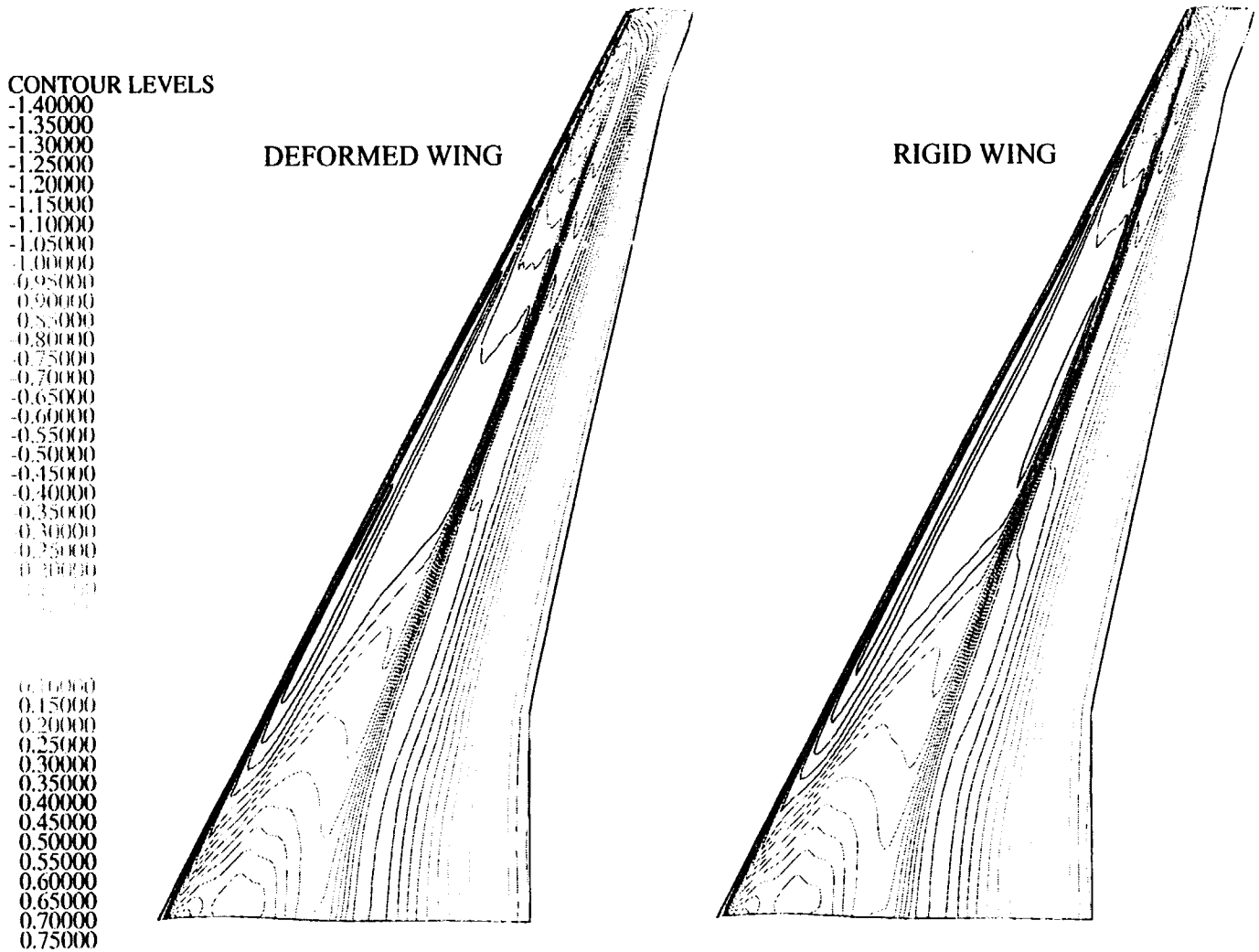

Figure 16. The pressure contours of the MD-90 wing under the cruise condition

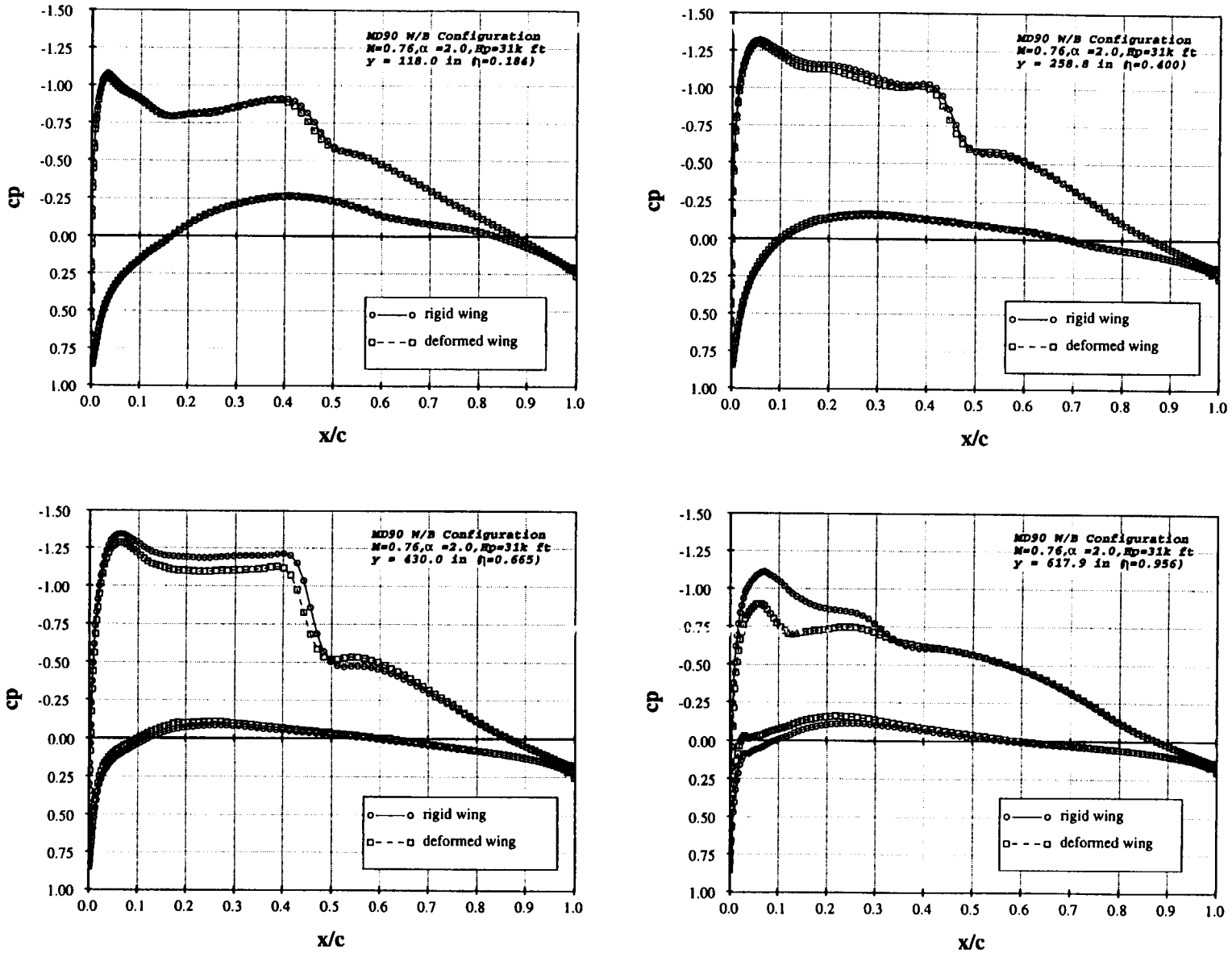

Figure 17. The pressure distributions at four spanwise locations of the MD-90 wing under the cruise condition

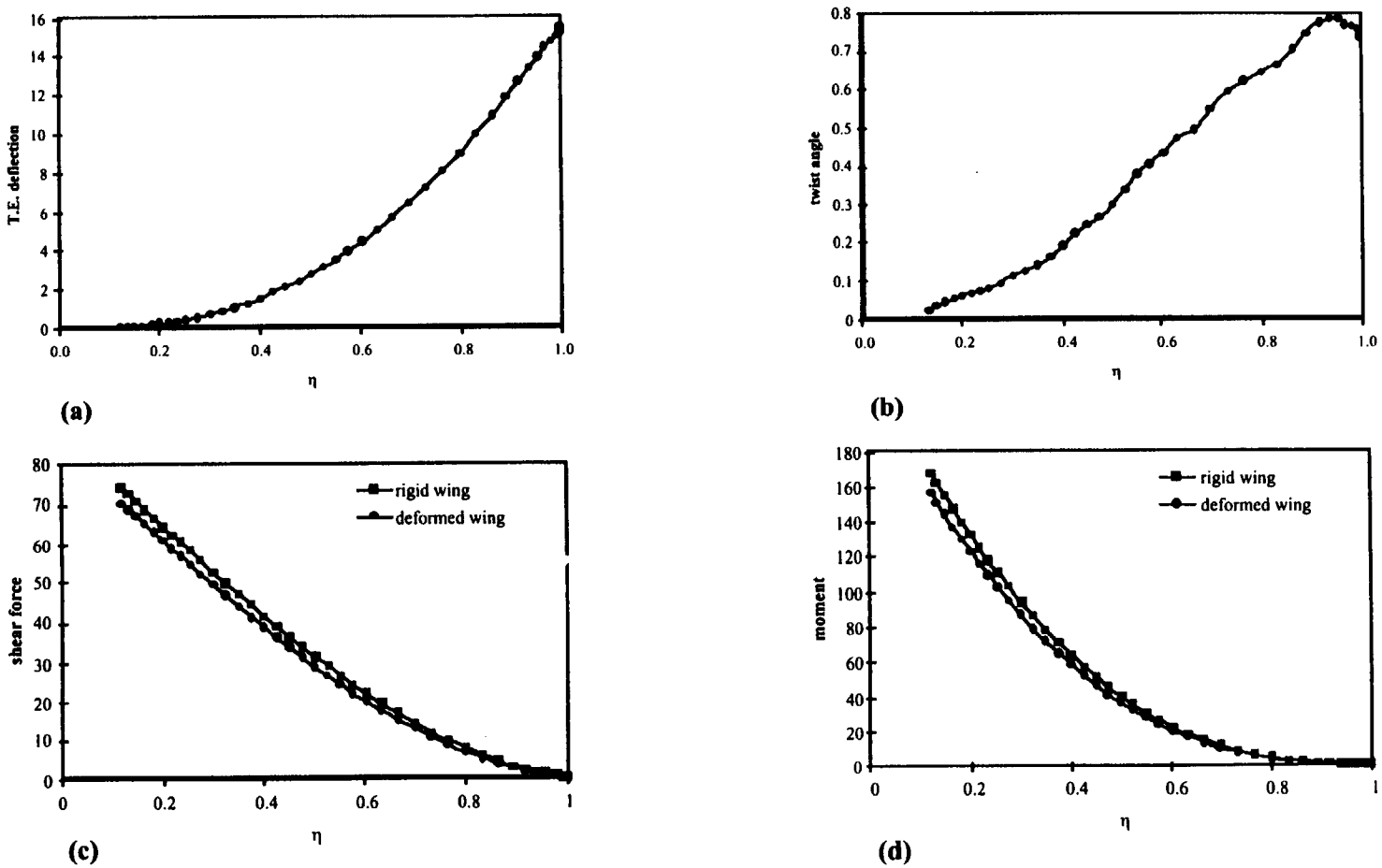

Figure 18. (a) The trailing edge deflection (b) the elastic twist angle (c) the shear force distribution and (d) the bending moment distribution of the MD-90 wing under the cruise condition